Comparative wind tunnel study of ice-shedding properties of bridge cables with wire meshes

Test Report

DEPARTMENT OF ENGINEERING
AARHUS UNIVERSITY

DEPARTMENT OF ENGINEERING
AARHUS UNIVERSITY

Title of Report:

Comparative wind tunnel study of ice-shedding properties of bridge cables with wire meshes

Authors:	***Initials:***	***Signatures:***	***Date:***
Lubomir Matejicka	LM		2019-09-09

Revision	***Description***	***By***	***Date***

Keywords:	***Classification:***
ice accretion; ice shedding; helical fillets; ice retention; wire mesh	

Approved by:	***Initials:***	***Signatures:***
Christos T. Georgakis	CG	

Department of Engineering
Aarhus University
Inge Lehmanns Gade 10, DK-8000 Aarhus C
Denmark

Table of Contents

Introduction

Cable-supported bridges can be adversely affected by ice and snow accretions that develop in specific weather conditions, predominantly in cold climate regions. Besides the bridge deck and pylons, the bridge cables are prone to ice accretion due to their exposure. Ice not only modifies the aerodynamic properties of the cables but more importantly, poses a serious risk for traversing traffic and pedestrians. The problem occurs when the ice starts to melt and, consequently, sheds in sizable pieces. In such events, the authorities are usually forced to close the bridge until the risk has diminished. In addition to the measurable regional economic losses due to traffic congestion, and the financial losses of the local authorities due to damages and claims, the reputation of the bridge and its owner/operator might suffer as well.

Numerous anti-icing and de-icing technologies have been tested in laboratories as well as on bridges, but none have proven to be a viable and effective solution. As a part of an ongoing investigation aimed to mitigate the risk of ice shedding from bridge cables trough improved ice retention leading to prolonged melting of the ice, a series of wind tunnels test were undertaken. This test report presents preliminary results of a passive ice retention system in the form of a wire mesh attached to the surface of the cable, which can effectively reduce the risk associated with ice accretions. Due to the structure of this system, which is not an integral part of the stay cable sheathing, it is suitable for both new bridges as well as for the existing bridges. The ice-retention and ice-shedding performance of a conventional, helically-filleted, high-density polyethylene (HDPE) stay pipe is compared to pipes fitted with four different wire mesh configurations.

Materials and methods

Wind tunnel facility

The wind tunnel tests were performed at the 2 × 2 m^2 cross-section closed-circuit DTU/Force Climatic Wind Tunnel (CWT), located at Force Technology, Lyngby, Denmark. The maximum wind speed in the test section of the CWT is 31 m/s at a turbulence intensity I_u < 1.0 %. The core feature of the CWT is a 250 kW cooling unit capable of sustaining long-term freezing temperatures up to -10 °C in the test section. Details of the design specifications of the tunnel are outlined by Georgakis et al. (2009).

Cable sections

The tested cable sections were full-scale specimens of sections of HDPE stay cable sheathing. In total, five different cable sections with an outer cylinder diameter of 160 mm, length of 1.52 m and various geometry of surface-modifying protrusions/elements (Figure 1) were tested.

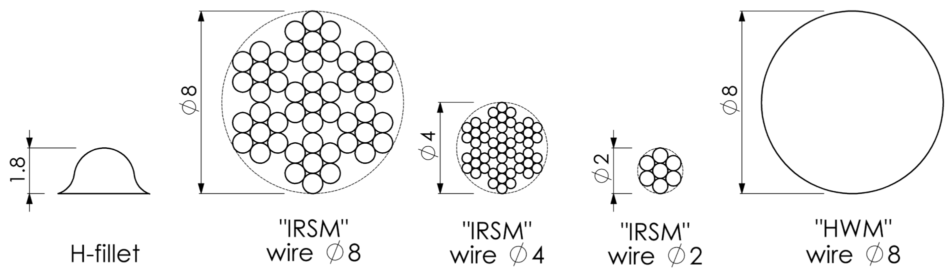

Figure 1: Tested fillets and wire profiles

The first, referential, cable section included the conventional stay pipe solution with semi-circular helical fillets (Figure 2a), further referred to as “H-fillet”. The average height of the fillets was 1.8 mm and the fillets were formed in a double-helical pattern with a helix angle of 45°.

The next three cable sections comprised retrofit solutions in the form of a steel wire mesh tautened on a plain cylinder. They are further referred to as “IRSM”, which stands for **I**ce **R**etention **S**teel **M**esh. The full denotation of the individual meshes includes a suffix referring to the number of wires, the diameter of the wires and the corresponding helix angle of the mesh. The first mesh utilized four 8 mm stainless steel wire ropes in an opposite double-helical pattern with a helix angle of 32° and is denoted as IRSM-4x8-32 (Figure 2b). Each individual wire rope was made up of steel cables with a 7x7 construction (a combination of seven strands composed of seven wires as shown in Figure 1). The other two steel wire mesh solutions were also formed with stainless steel wire ropes with diameters of 2 mm and 4 mm. The meshes consisted of six wire ropes in an opposite triple-helical pattern with a helix angle of 28°. They are denoted as IRSM-6x2-28 (Figure 2c) and IRSM-6x4-28 (Figure 2d).

The last cable section utilized a wire mesh that consisted of heating wires enclosed in a heat shrink tubing (Figure 2e). The geometry of this cable section was the same as IRSM-4x8-32 and its denotation is HWM-4x8-32, where “HWM” stands for **H**eating **W**ire **M**esh.

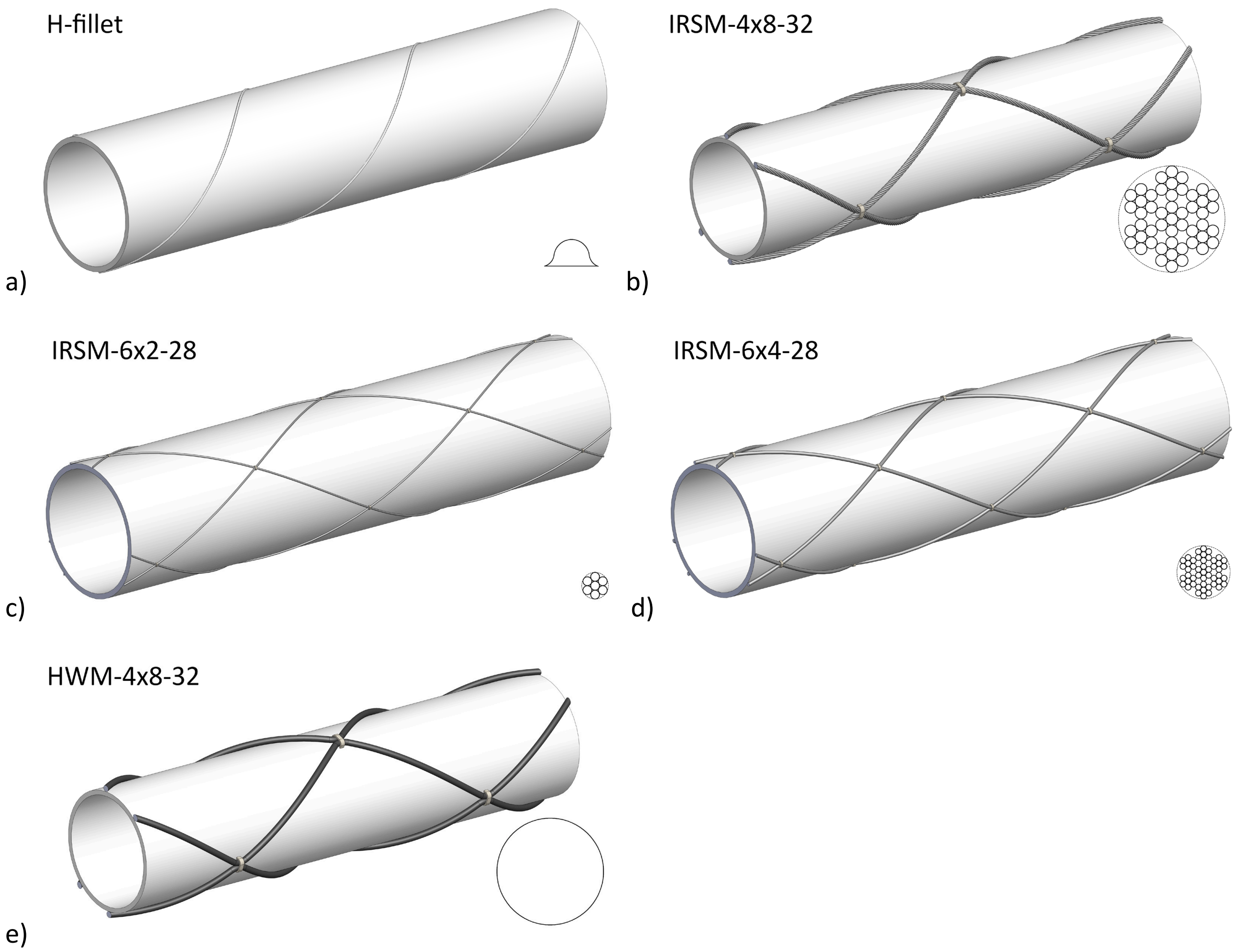

Figure 2: Tested cable sections

Test setup

One of the primary goals of the tests was to reproduce the formation of glaze ice on the cable surface. This was accomplished by controlled spraying of water on the cable sections at temperatures below 0 °C. For this purpose, two adjustable spray nozzles were installed in the test section through openings in the ceiling, approximately 2 m from the test specimen and 0.8 m from each other (Figure 3a). In order to create a uniform spray pattern along the cable axis, the spray nozzles were positioned in the test section at different heights corresponding to the cable inclination. The spray system was connected to a desalinated water supplier with a water pump supplying the water under a pressure of 4.0-4.1 bar, which resulted in the average water flow of 0.8 l/min. The nozzles produced an undefined spray pattern of fine mist.

The structural core of the test rig consisted of a 1.56 m long aluminum pipe with a diameter of 65 mm and a wall thickness of 1.5 mm. To center the position of the aluminum pipe inside the cable sections, a pair of custom-made nylon spacers was used at both ends of the pipe. Next, eight resistance silicone heating cables were equidistantly attached to the aluminum pipe in parallel to its axis (Figure 3b). The purpose of the heating cables was to simulate the heating effect of the solar radiation at the ice-surface interface. By heating the air inside the test specimen, the pipe surface was gradually heated up by the convective and conductive heat transfer. Basic specifications of the heating cables were a voltage of 230 V, a power usage of 36.8 W/m and a resistance of 230 Ω/m. The heating system was controlled by an electronic thermostat with a temperature sensor placed inside the test specimen.

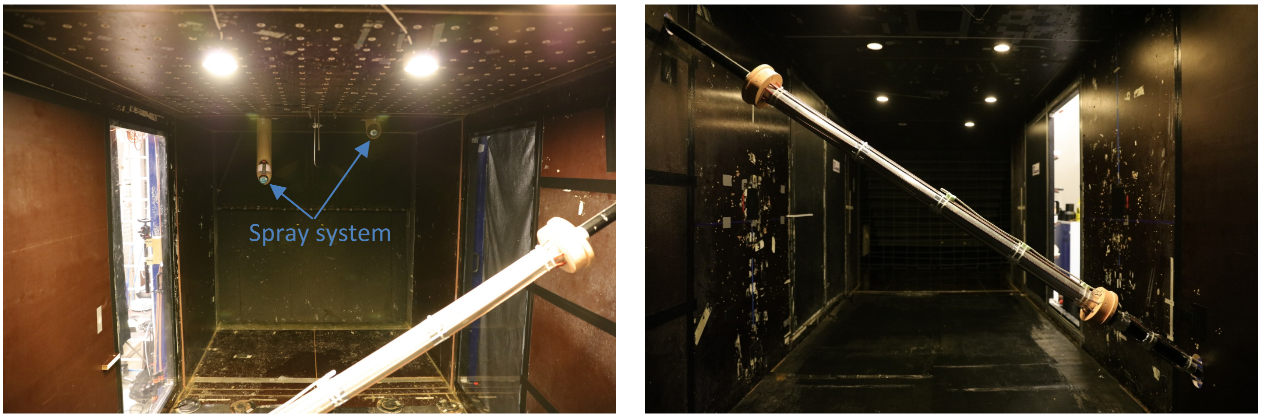

a) b)

Figure 3: Test assembly: a) spray nozzles; b) test rig

All the tests were performed on the cable sections installed at a constant yaw angle of 90° and an inclination of 33° (Figure 4a). The whole test rig with the test specimen was suspended from the load cells that were fixed to a rigid steel frame outside the test section to minimize the signal noise due to temperature and wind speed changes. As the inner aluminum pipe was not long enough, two additional steel pipes were used as extendable arms protruding outside of the test section through openings in the walls. Dummy pieces of HDPE sheathing of the same diameter as the cable sections were used to cover the parts of the extendable steel pipes within the test section. A hinge connection between the load cells and the suspended test rig was made by using eyebolts, steel hooks and nylon laces to connect them (Figure 4b). Both ends of the test specimen were sealed by plastic wrapping in order to prevent any water ingress into the pipe.

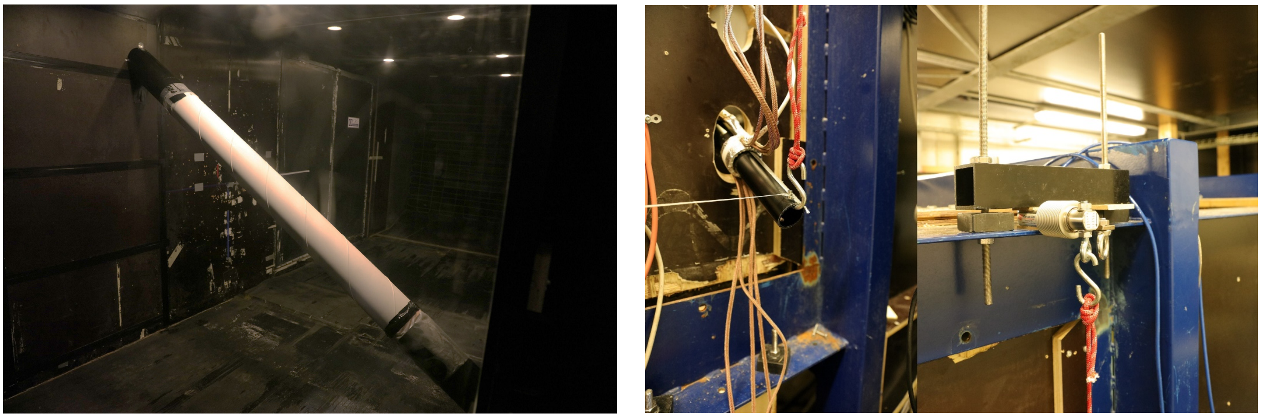

a) b)

Figure 4: Test setup: a) cable section installed at 33° inclination; b) hinge connection of the suspension system

Test method

As the parameters of the spray produced by the spray system were not defined, a set of trial tests was carried out to determine the conditions for creating glaze ice on the test specimen. Similarly to the previous tests performed by Matejicka et al. (2019), the specific liquid water content created by the spray system resulted in excess water running down the cable rather than freezing. Therefore, a method for operating the spray system in specific time intervals was also adopted for this experimental investigation. A graphical representation of the testing procedure is shown in Figure 7.

The cable section with H-filleted surface was used as a reference to determine the number of icing sequences. The aim of the trial tests was to reach ice accretion with an approximate mass of 1.5 kilograms of ice per meter of cable length. This corresponded to approximately 6-8 mm accretion thickness and icicle lengths of up to 150 mm. The mass of ice accretion was measured on a specific length of the tested cable section. Due to the end spacers, which had an insertion length of 50 mm, the heating cables inside the cable section covered only a length of 1.42 m, which was used to assess the mass of the ice accretion. Based on the trial tests, the replication of glaze ice was set to 24 sets of icing sequences. One icing sequence comprised two 1-minute intervals. The purpose of the first interval was to reproduce the atmospheric precipitation using the spray system. The second interval, during which the spray system was stopped, provided enough time for any excess runoff water to freeze. The raining intervals are represented by the grey columns in the ice accretion section of Figure 5.

As shown in Figure 5, the first step of every test was cooling the air temperature in the test section to -5 °C at a wind speed of 2 m/s. Once the temperature was reached, the wind speed was raised to 7 m/s, and the set of icing sequences was initiated. Once the last icing sequence finished, the wind speed in the test section was brought down to 2 m/s. From this point, the temperature in the test section was steadily increased to 0 °C. During this phase, any excess ice accreted beyond the effective heating length was removed and the ice accretion mass was measured. The ice-shedding phase started when the air temperature in the test section reached 0 °C. At the same time, the heating system was turned on and the time history of ice shedding was recorded. As this temperature was found insufficient in terms of test duration during the test of the steel wire mesh IRSM-4x8-32, further tests performed on “IRSM” samples were conducted at the air temperature of 2-3 °C.

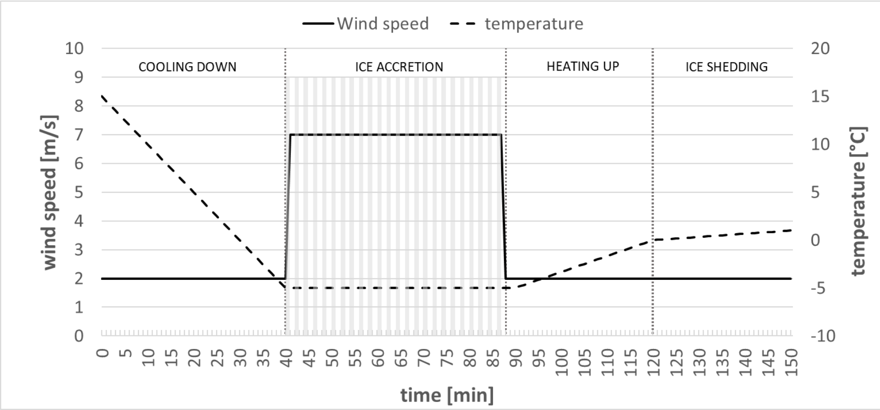

Figure 5: Time history of the ice-shedding test procedure, first 150 minutes

As the focus of this study was on the general ice shedding performance of the presented bridge cable surfaces at low wind speeds, no cable vibrations naturally occurring on bridges were reproduced. The reported results may change if large amplitude vibrations are taken into consideration.

Results

H-fillet, ice-shedding at 0 °C

a) b)

Figure 6: H-fillet: a) ice accretion; b) ice shedding

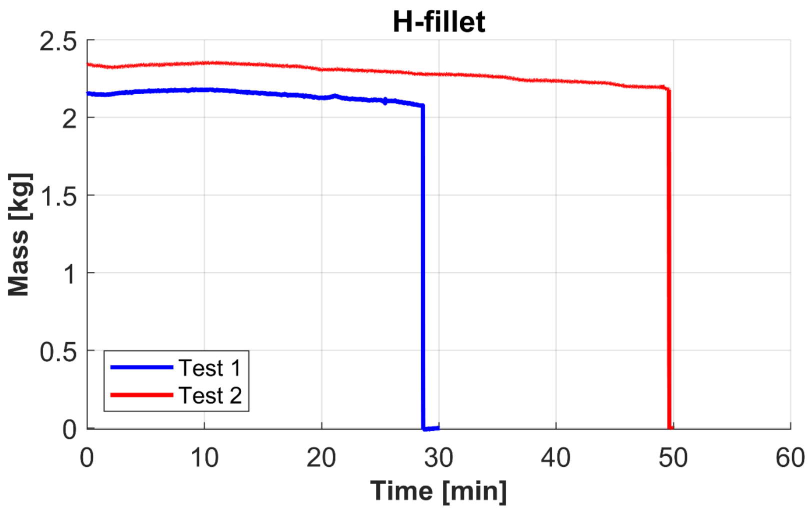

Figure 7: H-fillet: Time history of ice shedding

Table 1: H-fillet: Ice-shedding test statistics

	Ice accretion mass [kg]	Total shedding time [min]	Mass melted prior to shedding [%]	Melting time prior to shedding [min]	Number of shed ice pieces [-]	Mass of the heaviest shed ice piece [kg]
Test 1	2.15	29	3.3	29	1	2.08
Test 2	2.34	50	6.8	50	1	2.18

IRSM-4x8-32, ice-shedding at 0 °C

a) b)

Figure 8: IRSM-4x8-32: a) ice accretion; b) remaining ice accretion after 4 hours of ice melting

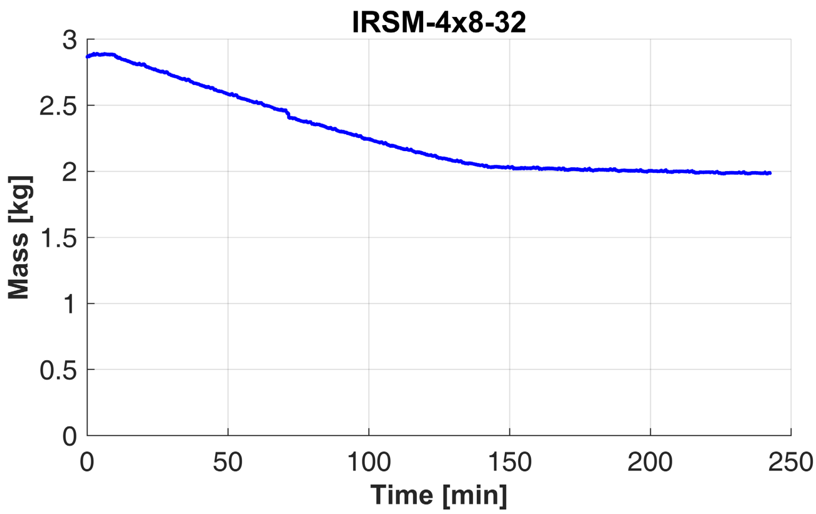

Figure 9: IRSM-4x8-32: Time history of ice shedding

Table 2: IRSM-4x8-32: Ice-shedding test statistics

	Ice accretion mass [kg]	Total shedding time [min]	Mass melted prior to shedding [%]	Melting time prior to shedding [min]	Number of shed ice pieces [-]	Mass of the heaviest shed ice piece [kg]
Test 1	2.87	240+	30.7*	240+	-	-

* No ice shedding was observed within the test time limit of 240 min. Therefore, this value corresponds to the mass melted within the time limit.

HWM-4x8-32, ice-shedding at 0 °C

a) b)

Figure 10: HWM-4x8-32: a) ice accretion; b) ice shedding

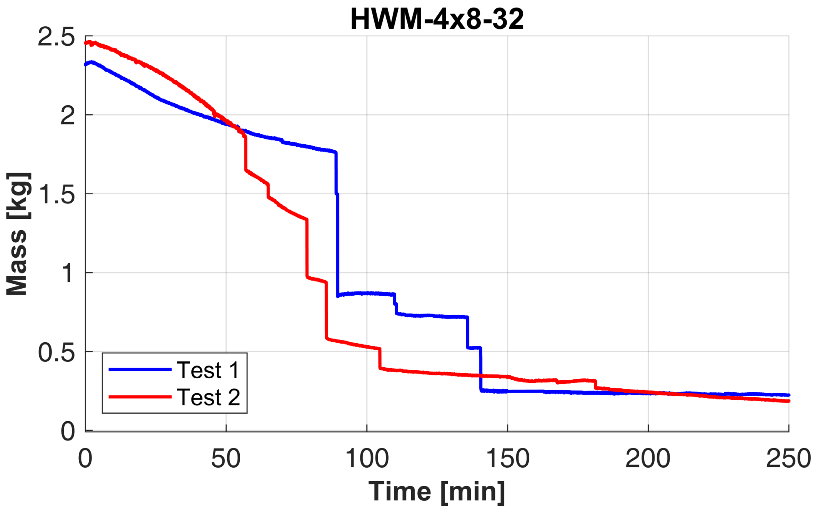

Figure 11: HWM-4x8-32: Time history of ice shedding

Table 3: HWM-4x8-32: Ice-shedding test statistics

	Ice accretion mass [kg]	Total shedding time [min]	Mass melted prior to shedding [%]	Melting time prior to shedding [min]	Number of shed ice pieces [-]	Mass of the heaviest shed ice piece [kg]
Test 1	2.32	240+	27.6	89	6	0.64
Test 2	2.45	240+	24.9	57	6	0.36

IRSM-4x8-32, ice-shedding at 2-3 °C

a)

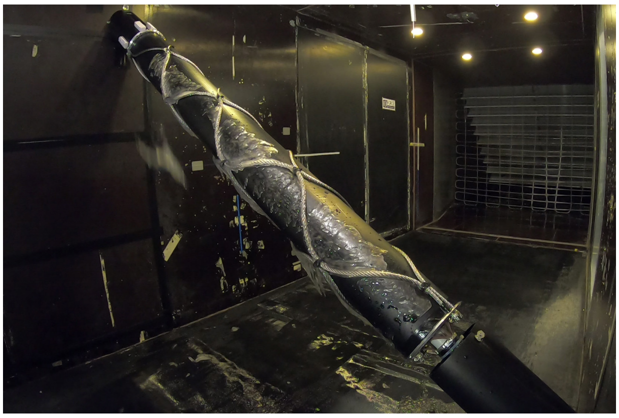

b)

Figure 12: IRSM-4x8-32: a) ice accretion; b) ice shedding

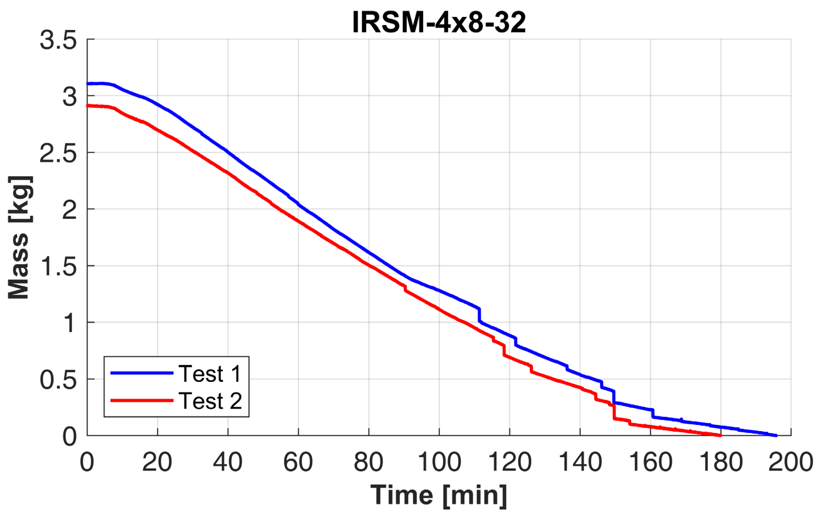

Figure 13: IRSM-4x8-32: Time history of ice shedding

Table 4: IRSM-4x8-32: Ice-shedding test statistics

	Ice accretion mass [kg]	Total shedding time [min]	Mass melted prior to shedding [%]	Melting time prior to shedding [min]	Number of shed ice pieces [-]	Mass of the heaviest shed ice piece [kg]
Test 1	3.10	195	63.9	111	7	0.11
Test 2	2.91	180	54.6	90	9	0.11

IRSM-6x2-28, ice-shedding at 2-3 °C

a)

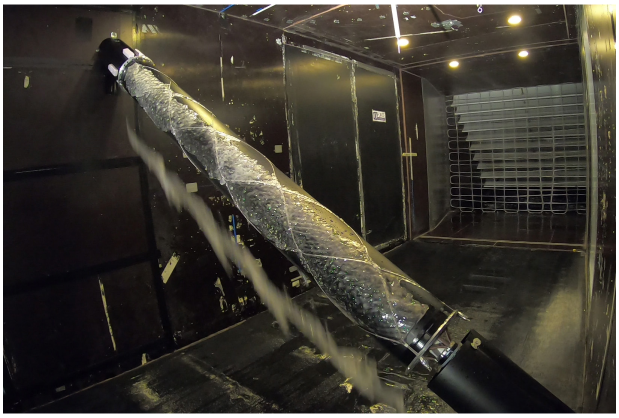

b)

Figure 14: IRSM-6x2-28: a) ice accretion; b) ice shedding

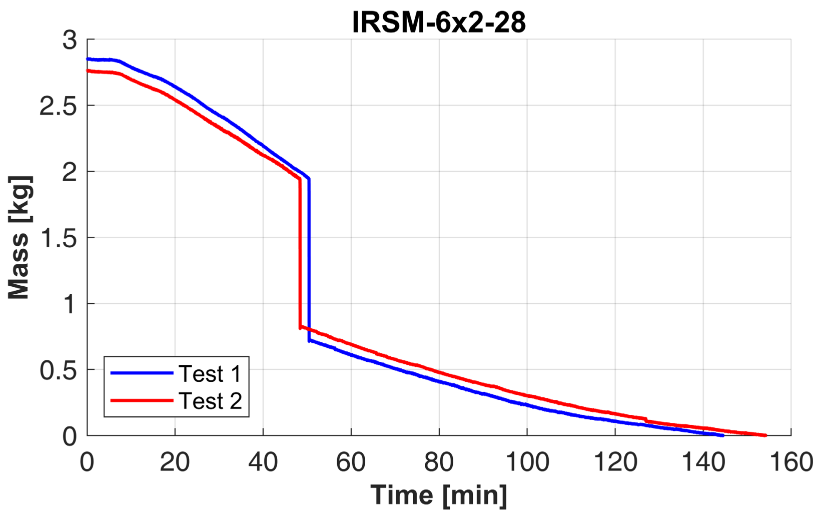

Figure 15: IRSM-6x2-28: Time history of ice shedding

Table 5: IRSM-6x2-28: Ice-shedding test statistics

	Ice accretion mass [kg]	Total shedding time [min]	Mass melted prior to shedding [%]	Melting time prior to shedding [min]	Number of shed ice pieces [-]	Mass of the heaviest shed ice piece [kg]
Test 1	2.85	144	31.9	50	1	1.22
Test 2	2.76	154	29.7	48	2	1.11

IRSM-6x4-28, ice-shedding at 2-3 °C

a)

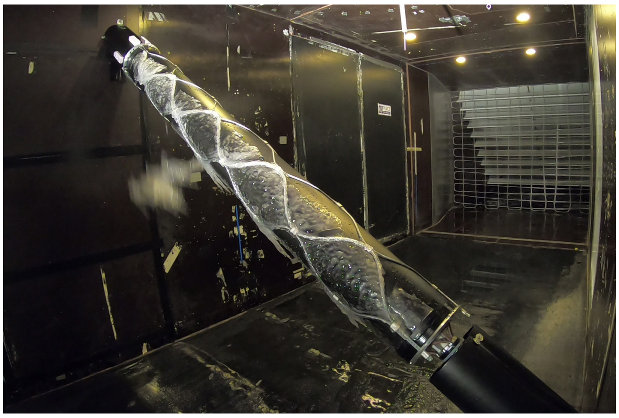

b)

Figure 16: IRSM-6x4-28: a) ice accretion; b) ice shedding

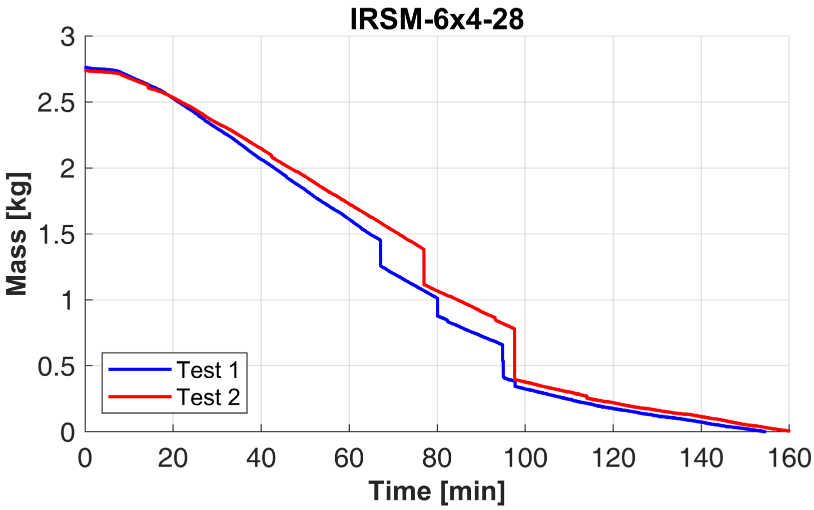

Figure 17: IRSM-6x4-28: Time history of ice shedding

Table 6: IRSM-6x4-28: Ice-shedding test statistics

	Ice accretion mass [kg]	Total shedding time [min]	Mass melted prior to shedding [%]	Melting time prior to shedding [min]	Number of shed ice pieces [-]	Mass of the heaviest shed ice piece [kg]
Test 1	2.76	154	47.5	67	4	0.20
Test 2	2.73	160	49.5	77	6	0.38

Comparison of results

The testing statistics and results of the ice-shedding tests are summarized in Table 7. Furthermore, a comparison of the tested cable sections within the individual result categories is presented in the form of column charts. The results in the column charts are ordered from the least to the most favorably performing cable surface in a given category based on the mean value of the compared parameter.

Table 7: Ice-shedding tests results

	Ice-shedding temperature 0 °C						Ice-shedding temperature 2-3 °C					
Cable surface \ Ice-shedding parameter	H-fillet		IRSM-4x8-32		HWM-4x8-32		IRSM-4x8-32		IRSM-6x2-28		IRSM-6x4-28	
	Test1	Test 2	Test1	Test 2	Test1	Test 2	Test1	Test 2	Test1	Test 2	Test1	Test 2
Ice accretion mass [kg]	2.15	2.34	2.87		2.32	2.45	3.1	2.91	2.85	2.76	2.76	2.73
Total shedding time [min]	29	50	240+	-	240+	240+	195	180	144	154	154	160
Mass melted prior to shedding [%]	3.3	6.8	30.7	-	27.6	24.9	63.9	54.6	31.9	29.7	47.5	49.5
Melting time prior to shedding [min]	29	50	240+	-	89	57	111	90	50	48	67	77
Number of shed ice pieces [-]	1	1	-	-	6	6	7	9	1	2	4	6
Mass of the heaviest shed ice piece [kg]	2.08	2.18	-	-	0.64	0.36	0.11	0.11	1.22	1.11	0.2	0.38

* No ice shedding was observed within the test time limit of 240 min. Therefore, this value corresponds to the mass melted within the time limit.

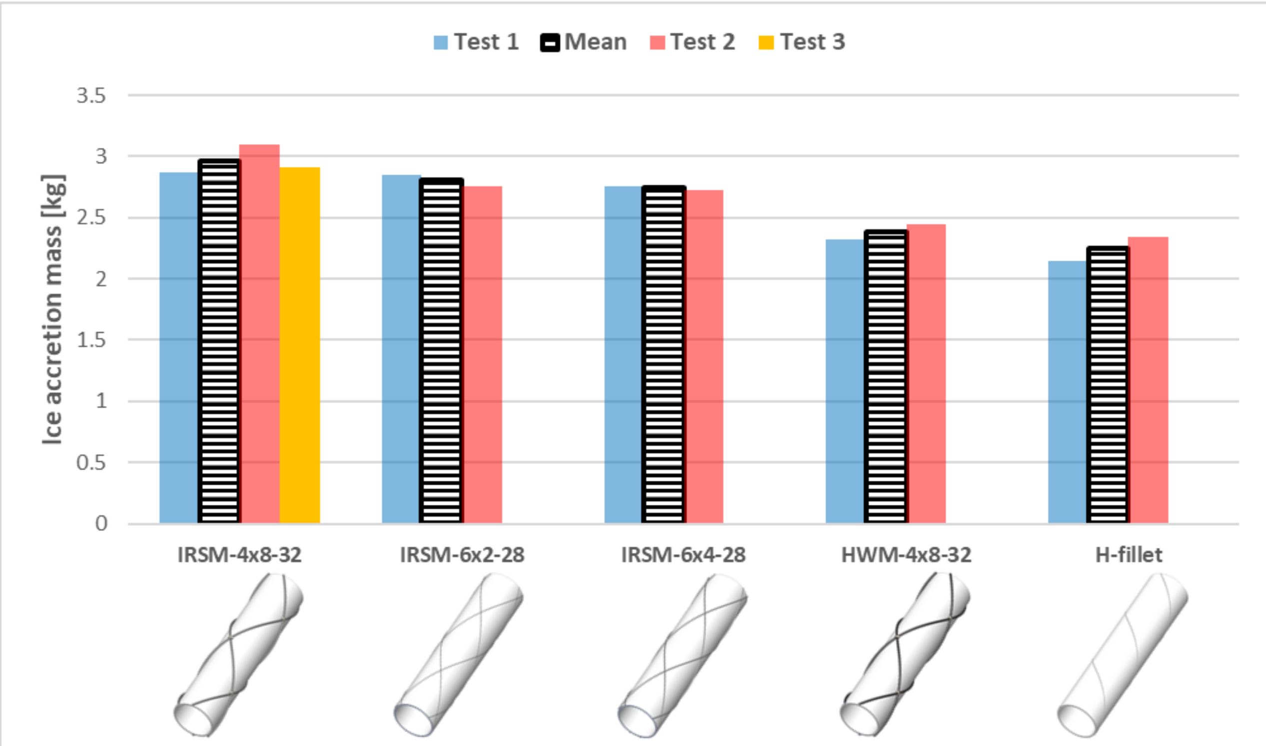

Figure 18: Ice accretion mass: mean value comparison

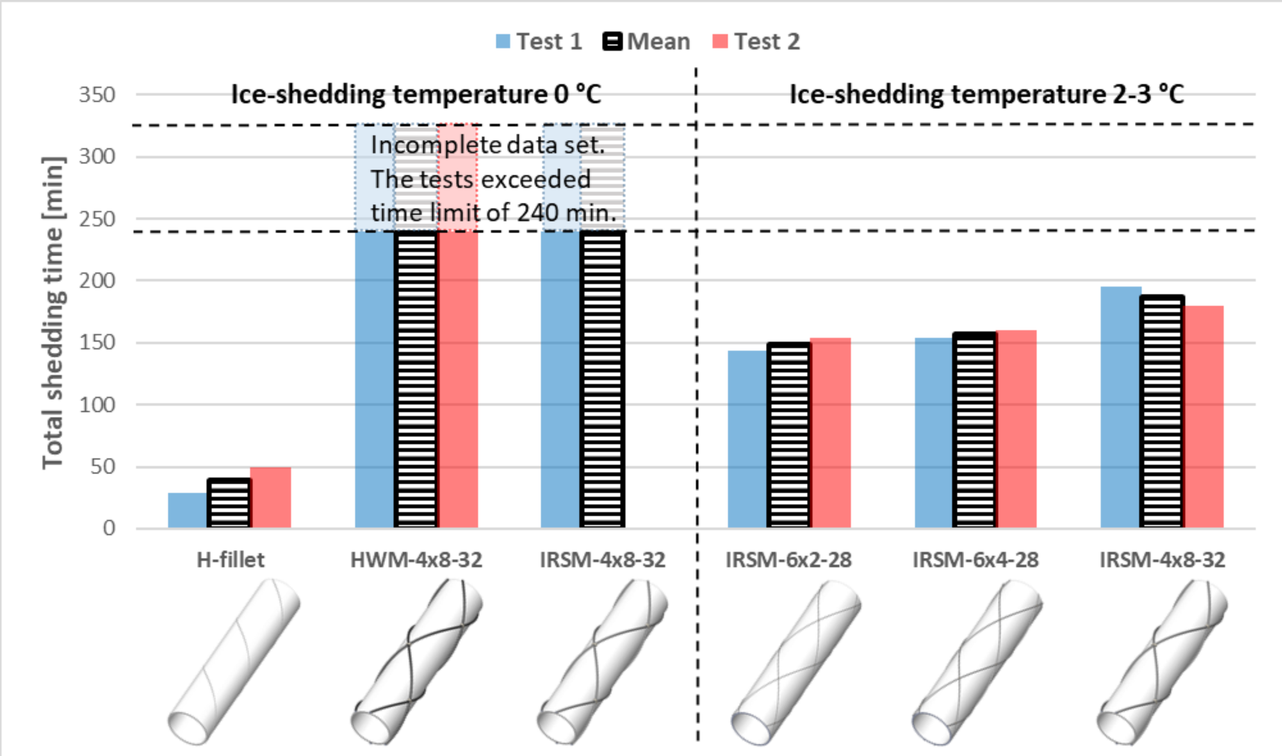

Figure 19: Total ice-shedding time: mean value comparison

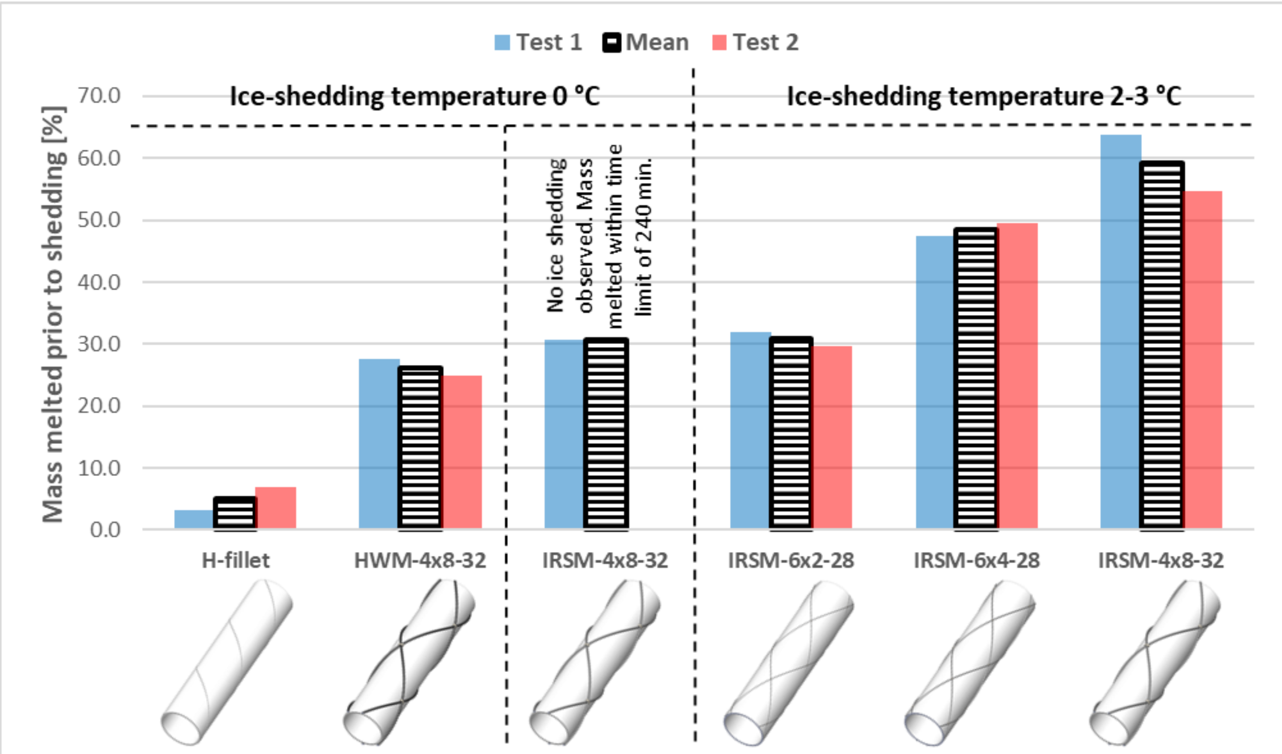

Figure 20: Ice mass melted prior to ice-shedding: mean value comparison

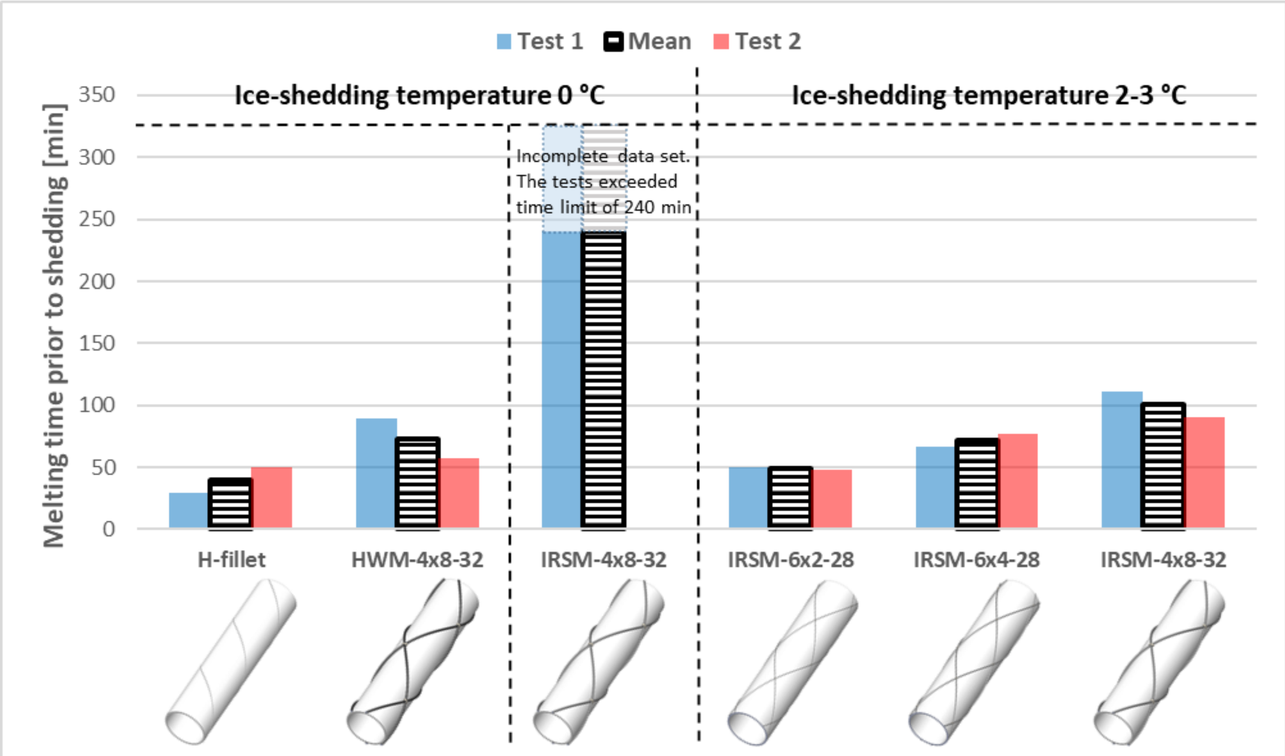

Figure 21: Melting time prior to ice-shedding: mean value comparison

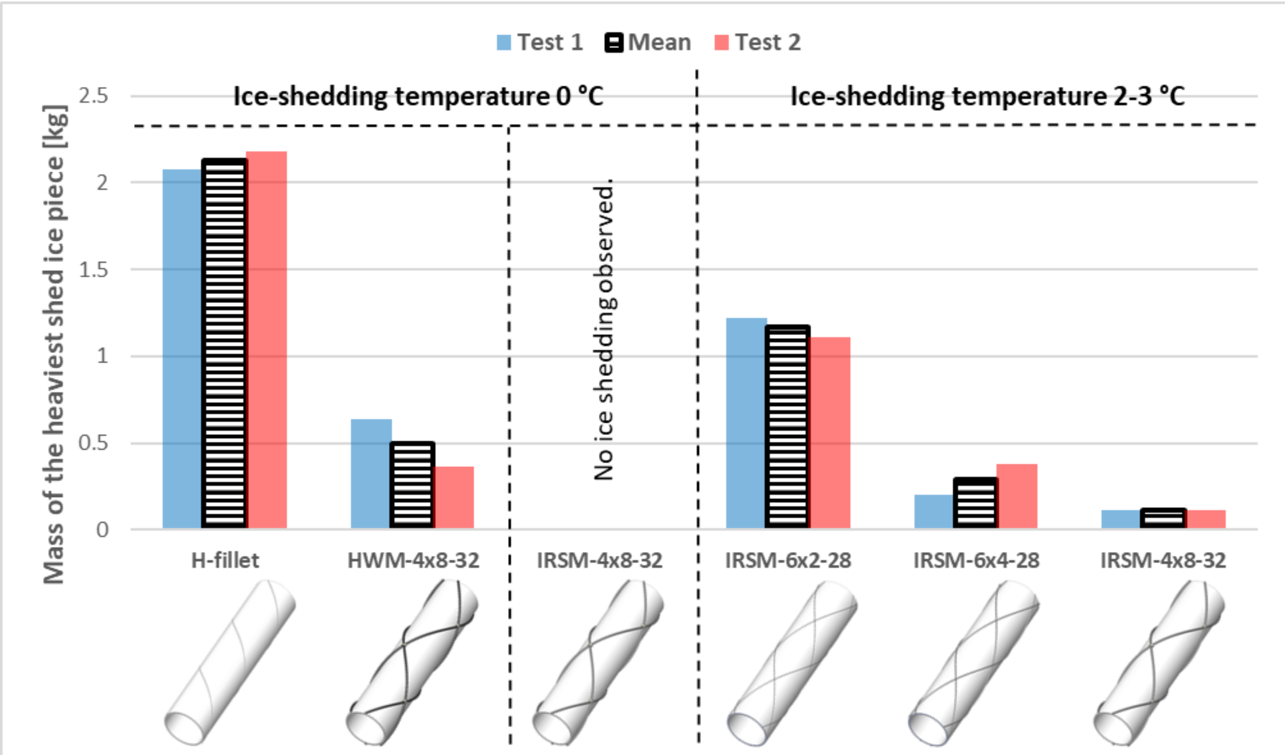

Figure 22: Mass of the heaviest shed ice piece: mean value comparison

Discussion of results

Two ice-shedding tests were undertaken in a climatic wind tunnel for each cable section, from which a few preliminary observations can be made. Henceforth a desirable or “good” performance refers to the ability of the cable surface to retain ice for an increased period of time while “poor” performance refers to the cables surface having no or minimum ability to retain ice. It should be noted that the higher ice-shedding temperature negatively affects the ice-shedding performance. It is therefore assumed that the cable sections tested at the lower ice-shedding temperature of 0 °C might exhibit a decrease in performance if tested at higher temperatures. The key ice-shedding parameters used for the comparison were based on time and mass measurements.

As can be seen from Figure 7, the conventional cable surface, H-fillet, shed the ice in one piece in both cases after a short period of time. Due to its poor ice retention capability and the relatively low ice-shedding temperature of 0 °C, which caused the low melting rate, the ice mass loss was only about 5 % of the originally accreted ice mass. Despite that, Figure 18 reveals that this cable section accreted the least amount of ice out of all tested cable sections. This performance corresponds well with the previous findings by Matejicka et al. (2019).

The results of HWM-4x8-32 show that this cable section was able to retain the ice for longer and break it into multiple pieces due to its geometry forming distinct areas of separation. The heaviest ice piece shed off the cable had 0.64 kg, which corresponds to about 28 % of the ice accretion mass. As this wire mesh consisted of heating wires not used during the tests, the performance could be further optimized by the employment of the heating system as an active anti- or de-icing system when needed.

A substantial improvement of the ice retention capability was shown by IRSM-4x8-32, which retained the ice accretion for the longest period of time at both ice-shedding temperatures. This allowed the ice retained on its surface to steadily melt and lose up to 64 % of its mass before it shed in multiple light pieces with a maximum mass of 0.11 kg. Although IRSM-4x8-32 outperformed all the other cable sections in the ice-shedding phase of the tests, it also accumulated the highest amount of ice.

The steel mesh with the smallest size of wires IRSM-6x2-28 was able to retain the ice for the shortest amount of time before shedding out of the cable sections with wire meshes. Despite this, the loss of ice mass prior to ice shedding amounted to about 30 %. Approximately 40 % of the mass corresponding to 1.1-1.2 kg was then shed off in one piece. The remaining ice accretion was retained on upper part of the cable section and melted away with minimum ice shedding.

Lastly, it was observed that IRSM-6x4-28 was able to shed the ice in multiple pieces and to retain the ice longer than IRSM-6x2-28, losing approximately half of the ice mass prior to shedding. The mass of the heaviest shed ice piece was 0.38 kg, corresponding to 14 % of the original ice accretion. Despite showing better ice-shedding performance than IRSM-6x2-28 in each category, it was still outperformed by IRSM-4x8-32. This indicates that the main geometrical feature affecting the ice retention capability and the ice-shedding behavior is the size of the surface-modifying protrusion, in this case the size of the steel wire.

Acknowledgements

This research was financially supported by VSL International Ltd. and FORCE Technology.

References

Georgakis, C.T., Koss, H.H., Ricciardelli, F., 2009. “Design specifications for a novel climatic wind tunnel for testing of structural cables”. In *8th International Symposium on Cable Dynamics*, Paris, France, pp. 333-340.

Matejicka. L., Georgakis, C.T., Schwarz, A., Egger, P., 2019. “Cable Surface for the Reduction of Risk Associated with Bridge Cable Ice Accretions”. *Structural Engineering International*, 29:3, pp. 425-432, DOI: 10.1080/10168664.2019.1597453.